Tunnelling and Underground Space Technology 49 (2015) 50–66

Contents lists available at ScienceDirect

Tunnelling and Underground Space Technology

journal homepage: www.elsevier.com/locate/tust

Internal forces of underground structures from observed displacements

Raul Fuentes *

School of Civil Engineering, University of Leeds, Leeds LS2 9JT, United Kingdom

ARTICLE INFO

Article history:
Received 13 August 2014
Received in revised form 5 January 2015
Accepted 7 March 2015
Available online 20 April 2015

Keywords:
Axial forces
Curvature
Moment distributions
Piles
Retaining structures
Soil/structure interactions
Tunnels

ABSTRACT

This paper presents a method that provides a solution to the long standing problem of calculating internal force distributions based on displacement measurements of piles, retaining walls and tunnels. It is based on the principle of virtual work and therefore, analytically correct in the linear elastic range, and works without the need of any boundary conditions.

The validation against multiple case studies, showcasing loading conditions including seismic, earth pressures, external loads, or sliding slopes in multiple ground conditions and construction processes, confirms its flexibility and applicability to any structure where displacements are observed. Although the validation presented here applies to bending moments and axial forces, the method is theoretically correct and applicable to other internal force distributions.

1. Introduction

The behaviour and structural design of underground structures is governed by the distribution of internal forces. Out of these internal forces, bending moments are most critical for structures supporting bending forces, such as laterally loaded piles and retaining walls, and subsequently for the amount of reinforcement that the structure must be provided with. In tunnels, axial forces are equally relevant, not for reinforcement considerations only, but to guarantee its stability as well. However, despite the importance of these internal forces, traditional monitoring techniques of these structures concentrate on measuring total or relative deformations to verify design assumptions rather than enabling direct conclusions about the governing internal forces of the structure itself.

This disconnection between monitoring and design parameters arises for two main reasons (Fuentes, 2012): lack of proven and widely accepted monitoring techniques to measure internal forces, especially bending moments, and the lack of a general method to translate displacement measurements into internal forces.

With regards to bending moments, and in response to the first of the above shortcomings, some have recently developed techniques using fibre optics that are capable of measuring bending moments or curvature indirectly (e.g. see Inaudi et al., 1998; Mohamad et al., 2010, 2011, 2012; Fuentes, 2012). However, this technique is still suffering from the fact that measurements are indirect – i.e. curvature is inferred from axial strains – and that in order to obtain other relevant parameters, such as displacements, a cumbersome double integration needs to be carried out. Nip and Ng (2005) illustrated the problems of this integration process based on beam theory and overcame this successfully defining multiple boundary conditions over a controlled pile test and applying an iterative process to calculate the integration constants and fitting parameters. However, due to these conditions, the method cannot be simply used for other structures where less control over the boundary conditions is present. Mohamad et al. (2011) used a numerical integration and boundary conditions of zero rotation and displacement at the wall toe, which were reasonable due to the depth of the wall under consideration. For less deep structures this assumption would be incorrect and hence further measurements, additional known boundary conditions or both must be provided. Furthermore, it must be noted that calculation of displacements from curvature provides only part of the total displacement as it ignores rigid body translations and rotations.

The second shortcoming, translating displacements into bending moments or curvature, has been, to date, challenging. It involves the double derivation of a fitted curve to the displacement profile that, as Brown et al. (1994) highlighted, often presents difficulties and errors that propagate through the double derivation process. In order to reduce these errors, multiple readings are needed and other boundary conditions need to be imposed in advance so that the results are acceptable. Hence, although satisfactory solutions have been provided in the literature, these

* Tel.: +44 0113 343 2282.
E-mail address: r.fuentes@leeds.ac.uk

http://dx.doi.org/10.1016/j.tust.2015.03.002
0886-7798/

Nomenclature

a_j	distance from toe of the structure to the position where the unit-load is applied
A	area of cross section of the structure
AIC	Akaike Information Criterion
$\mathbf{B_N}$, $\mathbf{B_M}$, $\mathbf{B_V}$, $\mathbf{B_T}$	matrices which elements are the integrals resulting from the application of the method corresponding to the normal, moment, shear and torsion internal force distributions respectively
C_0, C_1, C_j, C_n	coefficients of linear equation representing the internal force distribution of the real structure
$\mathbf{C_N}$, $\mathbf{C_M}$, $\mathbf{C_V}$, $\mathbf{C_T}$	arrays of coefficients defining the normal, moment, shear and torsion internal force distributions respectively
$d\delta$, $d\theta$, $d\rho$, $d\gamma$	small displacement of the real structure
E	Young's modulus
G	shear modulus
I	second moment of inertia of cross section
I_p	polar moment of inertia
$f_0(x), f_1(x), f_j(x), f_n(x)$	functions of linear equation representing the internal force distribution of the real structure
f_n	function under evaluation
$\hat{f}$	estimate of function
h	embedded length in retaining walls
H	retained height in retaining walls
k	number of field measurements of displacements for the real structure
L	structure length in retaining walls/piles
n	indication on the number of functions used to approximate the internal force distributions
$M(\varphi)$	bending moment of the tunnel
$M_{(j)1}(x)$	bending moment in the pile/retaining wall caused by the unit-load force
$M_{(j)1}(\varphi)$	bending moment in the tunnel lining caused by the unit-load force
N_1, M_1, V_1 and T_1	normal stress, bending moments, shear stress and torsion internal force distributions of the unit-load structure
N_{real}, M_{real}, V_{real} and T_{real}	normal stress, bending moments, shear stress and torsion internal force distributions of the real structure
$q(x)$	external pressure acting on retaining walls/piles
$q(\varphi)$	external pressure acting on tunnel lining
R	radius of tunnel
SSE	Sum of Square of Errors
t	tunnel lining thickness
x	distance from the toe of the retaining wall/pile
u	displacement of real structure in retaining walls/piles
$\mathbf{u}$	array of field Observed displacements in retaining walls/piles
u_j	displacement of the real structure at the point j where the unit-load is applied
u_D	bending component of field measurement displacements in retaining walls/piles
u_D	lateral displacement of pile/retaining wall causing bending moments or radial component of distortion displacement at a point of the tunnel lining
u_C	uniform convergence displacement
u_O	observed lateral displacement of pile/retaining wall, radial displacement of the tunnel lining in the rotated tunnel
u_O^{SL}	radial displacement at the tunnel springline observed
u_{RB}	radial component of rigid body displacement at a point of the tunnel lining
u_{RB}^{SL}	radial component of rigid body displacement at the tunnel springline
u_D^{SL}	radial component of distortion displacement at the tunnel springline
u_O^{CR}	radial displacement at the tunnel crown observed
u_{RB}^{CR}	radial component of rigid body displacement at the tunnel crown
u_D^{CR}	radial component of rigid body displacement at the tunnel crown
u_{real}	field Observed displacements in retaining walls/piles
α_s	shear coefficient
β_j	angle measured from the vertical direction clockwise to the point of application of the unit-load
δ	translation displacement
φ	angle measured from the vertical direction at the tunnel crown and clockwise
ψ	rigid body rotation

apply to specific conditions and structures and therefore, need to be used with caution elsewhere.

The situation in tunnels is even more problematic as the available solutions to obtain bending moments and axial loads from displacements involve back-calculation and iterative processes using models that are successful in forward prediction – e.g. continuum models (Muir Wood, 1975; Curtis, 1976; Einstein and Schwartz, 1979; Duddeck and Erdmann, 1985; El Naggar et al., 2008; Carranza-Torres et al., 2013), convergence-confinment methods (e.g. Panet and Guenot, 1982), bedded beam springs (ITA, 1988; Oreste, 2003) or finite element analysis. Although satisfactory in its forward use, they also apply to specific conditions and still do not provide an independent check on the original calculation method.

This paper presents the first application of the unit-load to the calculation of internal forces – You et al. (2007) used its more typical application for displacement calculations for a shield tunnel and, similarly, Kim (1996) used it for validating the displacements obtained from predictive methods in model tunnels. It is based on the principle of virtual work, and enables calculating the internal force distributions of piles, retaining walls and tunnels when the displacements of the structure are known, without the need of any boundary conditions. The validation here concentrates on bending moments for all three structure types and axial forces in tunnels, as they are the most relevant to their performance. However, the methodology would equally apply to other internal force distributions.

2. The unit-load method in its traditional use

The unit-load (UL) method uses the principle of virtual work and is widely used in structural engineering for the calculation of displacements of structures. Its implementation involves the definition of two structural systems: one comprising the real structure with its external loads (denoted here as 'real') and the second (denoted as '1') consisting of the same structure with only a single unit-load applied at the point and in the direction of the displacement to be calculated. Once the two systems are defined, Gere and Timoshenko (1987) show that the displacement, u, of the real structure at the point of application of the unit-load is

$$u = \int N_1 d\delta + \int M_1 d\theta + \int V_1 d\rho + \int T_1 d\gamma \tag{1}$$

where N_1, M_1, V_1 and T_1 are respectively the normal stress, bending moments, shear stress and torsion internal force distributions of the unit-load structure. The second term in each integral represents the corresponding small displacement of the real system.The above equation applies to any material behaviour as long as the displacement terms are small (Gere and Timoshenko, 1987). For a linear elastic material, where the deformations are related to the internal forces through well-known elasticity constants, it becomes

$$u = \int \frac{N_1 N_{real}}{EA} dx + \int \frac{M_1 M_{real}}{EI} dx + \int \frac{\alpha_s V_1 V_{real}}{GA} dx + \int \frac{T_1 T_{real}}{GI_p} dx \tag{2}$$

where E is the elastic Young's modulus, G the shear modulus, I the second moment of inertia, A, the area of the cross section and I_p the polar moment of inertia.

3. Proposed method

Reversing Eq. (2) allows calculation of the internal forces of the real structure, N_{real}, M_{real}, V_{real} or T_{real}, based on the observed displacements, u, at a given time.

If N_{real}, M_{real}, V_{real} or T_{real} adopt a generalised linear equation of the form

$$\mathrm{N_{real}, M_{real}, V_{real}, T_{real}} = f(x) = C_0 + C_1 f_1(x) + C_2 f_2(x) + \ldots + C_n f_n(x) \tag{3}$$

the constants C and integrals can be separated and Eq. (1) can be written in its matrix form

$$\boldsymbol{u} = \boldsymbol{B_N} \cdot \boldsymbol{C_N} + \boldsymbol{B_M} \cdot \boldsymbol{C_M} + \boldsymbol{B_V} \cdot \boldsymbol{C_V} + \boldsymbol{B_T} \cdot \boldsymbol{C_T} \tag{4}$$

where the different suffices refer to each of the internal force distributions; $\boldsymbol{u}$ is the array containing all of the observed displacements, generally of dimensions (k,1); $\boldsymbol{C}$ $(n+1,\ 1)$ are single column arrays containing the coefficients in (3) that define the distributions of internal forces; and $\boldsymbol{B}(k, n+1)$ are matrices which elements are the integrals resulting from the application of Eq. (1) generally or (2) for linear elastic materials.Hence, Eq. (4) represents the general system of equations to be solved for $\boldsymbol{C}$. It must be noted that a different n may apply, in principle, for each internal force distribution (e.g. using the same number of coefficients for all distributions results in $4(n+1)$ unknowns). However, if only bending moments are considered, (4) can be written as

$$\begin{bmatrix} u_1 \\ u_2 \\ \cdots \\ u_j \\ \cdots \\ u_k \end{bmatrix} = \begin{bmatrix} \int \frac{M_{(1)1}}{EI} dx & \int \frac{M_{(1)1} f_1(x)}{EI} dx \ldots & \int \frac{M_{(1)1} f_i(x)}{EI} dx \ldots & \int \frac{M_{(1)1} f_n(x)}{EI} dx \\ \int \frac{M_{(2)1}}{EI} dx & \int \frac{M_{(2)1} f_1(x)}{EI} dx \ldots & \int \frac{M_{(2)1} f_i(x)}{EI} dx \ldots & \int \frac{M_{(2)1} f_n(x)}{EI} dx \\ \int \frac{M_{(j)1}}{EI} dx & \int \frac{M_{(j)1} f_1(x)}{EI} dx \ldots & \int \frac{M_{(j)1} f_i(x)}{EI} dx \ldots & \int \frac{M_{(j)1} f_2(x)}{EI} dx \\ \int \frac{M_{(k)1}}{EI} dx & \int \frac{M_{(k)1} f_1(x)}{EI} dx \ldots & \int \frac{M_{(k)1} f_i(x)}{EI} dx \ldots & \int \frac{M_{(k)1} f_n(x)}{EI} dx \end{bmatrix} \begin{bmatrix} C_0 \\ C_1 \\ \cdots \\ C_j \\ \cdots \\ C_n \end{bmatrix} \tag{5}$$

where $M_{(j)1}$ is the unit-load bending moment distribution of the system with a unit-load applied at the position and in the direction of u_j.

Each row in Eq. (5) can hence be rewritten as

$$u_j = \frac{1}{EI} \sum_{i=1}^{n+1} B_{ij} C_{i-1} \tag{6}$$

where $B_{i,j}$ represents each of the integrals shown in Eq. (5).

The system of equations in (5) was solved in MATLAB (2013) using the method of least-squares. The conditions for the system to have a unique solution are that $k > n+2$ and the rank of $\boldsymbol{B}$ is greater than k. In general the first condition will always apply (e.g. for a pile under lateral load where its bending moment is approximated using a 4th order polynomial, $n = 5$, k must be equal or greater than 7. This requirement is easily fulfilled in practice as the typical number of readings for an instrumented pile will traditionally exceed this number; the same typically applies to retaining walls and tunnels). The second condition was always fulfilled for the cases studied and should always be checked.

4. Application to retaining walls and laterally loaded piles

4.1. Assumptions

The following general assumptions are made: linear elastic material behaviour applies; cross sections that are plane before deformation remain plane and; only small deformations are applied to the structure.

Since the focus for piles and retaining walls is on calculating bending moments, only the displacements perpendicular to the pile/retaining wall longitudinal axis need to be considered.

It is also assumed that bending moments are the dominating internal force in relation to the above displacement and therefore, Eqs. (5) and (6) apply. This has been previously confirmed by others like Anagnostopoulos and Georgiadis (1993), who showed that the axial load has a limited effect on the lateral displacement of piles and concluded that it can be disregarded in static conditions, or Abdoun et al. (2003) who also confirmed this when showing that the presence of axial forces had little impact on lateral displacements under seismic loading. Similarly, shear forces can be disregarded as Gere and Timoshenko (1987) proved that their contribution to the lateral displacements is small. Finally, the problems studied here are either plane strain or axisymmetrical approximations, which means that torsion is also not relevant.

In order to apply (5) and (6), the real structures were idealised: propped walls as a simply supported beam (Fig. 1a) and cantilever walls and laterally loaded piles as a cantilever beam (Fig. 1b). Although these assumptions have been made by others – e.g. Nip and Ng (2005) for laterally loaded piles – they are proposed and their validation is part of this paper for more general conditions and geometries.

Structural observed displacements (herein called u_O – See Fig. 1c) can be divided into three different main components (Gaba et al., 2003): rigid body rotation (ψ); rigid body translation (δ) and; bending (u_D) as illustrated in Fig. 1d. Out of the three, only the latter contributes to the bending moments in the structure; hence, its isolation is needed for the application of the method and should be the only component to be used. In linear elastic behaviour, these can be superimposed which simplifies the process of sorting.

4.2. Formulation

Using polynomials of order n in Eq. (3) such as

$$f_0(x) = 1, f_1(x) = x^1, \ldots, f_n(x) = x^n \tag{7}$$

and the unit-load bending moment distributions for propped walls

$$M_{(j)1}(x) = \begin{cases} \frac{L-a_j}{L} x, & x < a_j \\ -\frac{a_j}{L} x + a_j, & x \geqslant a_j \end{cases} \tag{8}$$

and, similarly, for cantilever walls and laterally loaded piles (see Fig. 1 for variable definitions),

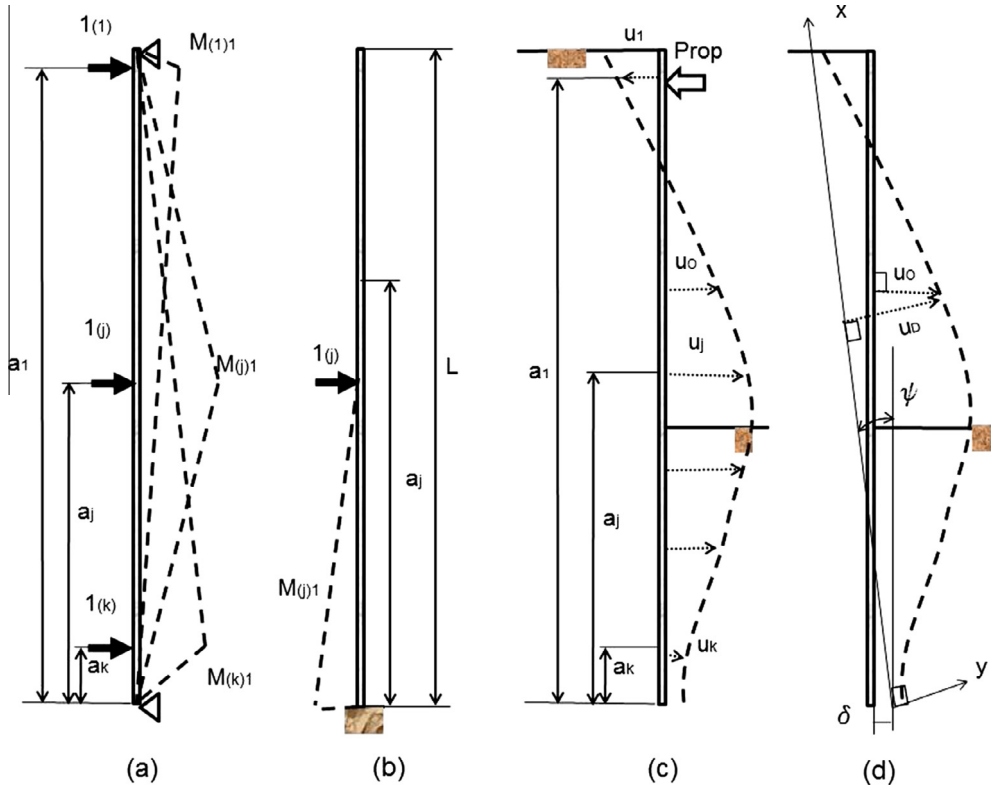

Fig. 1. Piles and embedded retaining walls (a) UL for propped walls, (b) UL for propped walls for cantilever walls and laterally loaded piles, (c) displacement definitions and (d) bending displacements.

$$M_{(j)1}(x) = \begin{cases} a_j - x, & x < a_j \\ 0, & x \geqslant a_j \end{cases} \tag{9}$$

the integrals in Eqs. (5) and (6) become

$$B_{j,i} = \frac{L - a_j}{L}\frac{a^{i+2}}{i+2} + a_j\left(-\frac{L^{i+1}}{i+2} + \frac{L^{i+1}}{i+1} + \frac{a_j^{i+2}}{(i+2)L} - \frac{a_j^{i+1}}{i+1}\right) \tag{10}$$

for propped retaining walls and

$$B_{j,i} = a_j\frac{a_j^{i+1}}{i+1} - \frac{a_j^{i+2}}{i+2} \tag{11}$$

for cantilever walls and laterally loaded piles.

Eqs. (10) and (11) define the system of equations in (5) and (6) to be solved.

4.3. Choice of function f(x)

Multiple authors have chosen polynomials to approximate displacements and bending moments of underground structures due to their versatility. However, the choice of order is much less thoroughly explained in the literature and the reasons for choice are normally justified by the amount of boundary conditions available, or a trial and error procedure rather than a rigorous goodness-of-fit. A common mistake is to choose higher order polynomials as they provide an apparent better fit to data; however, this may lead to over-fitting and instabilities that are important, especially if the polynomials are used to derive other parameters from its derivatives such as shear forces or soil reaction. de Sousa Coutinho (2006) proposed a sophisticated technique using polynomial splines in order to solve this problem. The strategy proposed here to address the above problem is simple and presented using Reese (1997) and Mohamad et al. (2011) case studies (see Table 1 for description):

- First, the bending moments are calculated using multiple polynomial orders and Eqs. (5), (6), (10) and (11). Typical starting values of polynomial orders, based on experience, are: 5th to 9th (Singly Propped walls), 6th to 10th (Multi-propped walls) and 4th to 8th (Cantilever walls and laterally loaded piles). The above values of polynomial order are only initial; iterations beyond those values may be necessary until the best order is found as shown below.
- Model Evaluation – The Akaike Information Criterion (AIC) (Akaike, 1974) was used to evaluate each polynomial. Later updates (Hurvich and Tsai, 1991), that correct for models where the number of points is similar to the number of independent variables to be estimated, were dismissed as it increases the risk of under-fitting (Bozogan, 1987). The AIC approach provides a formulation that complies with the principle of parsimony, by which the simplest model is selected, and eliminates the risk of over-fitting. AIC is found using the following equation

$$\mathrm{AIC} = -k * \mathrm{LN}\left(\frac{\mathrm{SSE}}{k}\right) + 2(n+1) \tag{12}$$

where SSE is the Sum of Square of Errors defined as

$$\mathrm{SSE} = \sum_{1}^{N}(f_n - \hat{f})^2 \tag{13}$$

and f_n is the polynomial under evaluation, and $\hat{f}$ is an estimator which is defined as the average of all the polynomials used.

Figs. 2 and 3 show the implementation of Eq. (5) and this strategy. The optimal orders (lowest AIC score) are 9th for Mohamad et al. (2011) and 6th for Reese (1997). When the lowest AIC value

Table 1
Case studies description.

Reference	Loading condition	Ground conditions*	Structure description & dimensions	Length (m)	EI (kN/m^2)	Comments
Retaining walls and piles						
Mohamad et al. (2011)	Multi-propped wall – bottom-up construction	Sand and gravels (5 m approx.) overlying London clay	Bored secant piled wall. Male piles of 0.508 m dia. at 600 mm spacing. Excavation depth – 10 m Three levels of temporary support	20.0	N/A	Curvature inferred by authors from fibre optic sensors located within the pile longitudinal reinforcement assuming elastic behaviour Displacement readings were obtained from inclinometer readings
Ou et al. (1998)	Multi-propped wall – top-down construction	From top to bottom: Silty clay (5.6 m) – silty sand (2.4 m) – Sitly clay (25 m) – Medimum dense fine sand (2 m) – Medium to stiff clay (2.5 m) – Medium to dense silty sand (8 m)	Diaphragm wall, 0.9 m thick. Excavation depth – 19.7 m	35.0	1.458E06**	Displacement readings were obtained from inclinometer readings Observed bending moments were calculated by the authors using longitudinal strain along the rebars
Reese (1997)	Pile loaded laterally at the pile head	From top to bottom: Sand (3.5 m) – Limestone (to depth)	Bored pile 1.22 mmΦ	6.39 (see comments)	3.73E06*	Instrumented model pile. The length was taken to the position where zero bending moments were provided by the authors It was assumed that the deformation of the pile was zero below the zero point shown in the Figure
Cheng et al. (2007) and Loganathan et al. (2000)	Laterally loaded piles from nearby tunnel construction	Kaolin Clay throughout	Hollow pile of 800 mm external and 724 mm internal dia	18.0	6.62E05*	Results from FE (Cheng, 2007) and centrifuge testing (Loganathan et al., 2000) FE calculated displacement readings were used as input
Liyanapathirana and Poulos (2005)	Earthquake induced lateral loading including liquefaction	Centrifuge test of model piles/ Saturated Nevada Sand with medium-dense overlying dense sand	Hollow circular 6061-T6 Aluminium (Wilson, 1998) section, 0.67 m dia., and 72.4 mm wall thickness	18.8	59,8578.2**	Bending moments were provided via the presented method by the authors EI was calculated from values of moment of inertia, $I = \pi R^3 t$, where R is radius of pile and t is wall thickness and E = 70 MPa
Smethurst and Powrie (2007)	Lateral soil pressure applied on piles installed in an embankment	From top to bottom: Imported fill – Weald Clay (WC) fill – Weathered WC – Intact WC	Bored piles 0.6 m dia. at 2.4 m spacing	10.0	1E05*	Displacement readings were obtained from inclinometer readings
Tunnels						
Reference	Loading condition	Ground conditions*	Structure description & dimensions	Radius (m)	EI (kN/m^2)	Comments
Carranza-Torres et al. (2013)	Idealised tunnel construction with ground loading only	Idealised elastic soil conditions with relaxation parameters	Concrete lining with a thickness of 0.5 m	5.0	26,0416.7**	EI was calculated from values of moment of inertia, $I = t^3/12$, where t is the lining thickness and E = 2.5 GPa
Brinkgreve et al. (2011)	Tunnel excavated in medium soft soil in the vicinity of a building founded on piles	From top to bottom: 13 m Soft clay (13 m) – Fine sand (2 m) – Firm clay (5 m) – Medium-Dense sand (13 m)	Concrete lining with a thickness of 0.35 m	2.5	1.43E05*	EA is provided and has a value of 1.47E07 kPa

* From ref.
** Inferred.

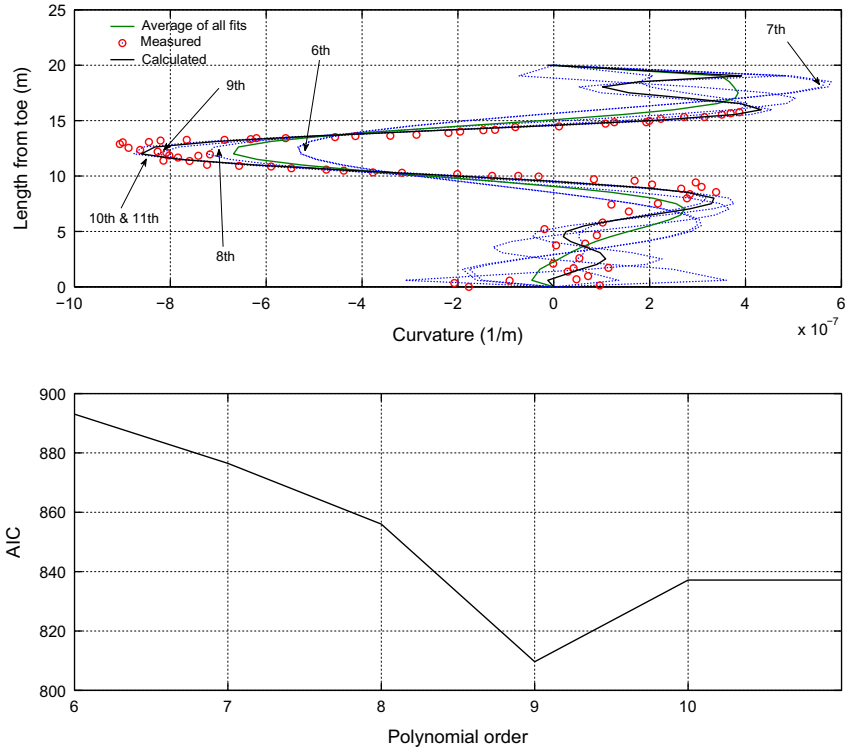

Fig. 2. Development of method for Mohamad et al. (2011) (a) Polynomial choice and (b) AIC.

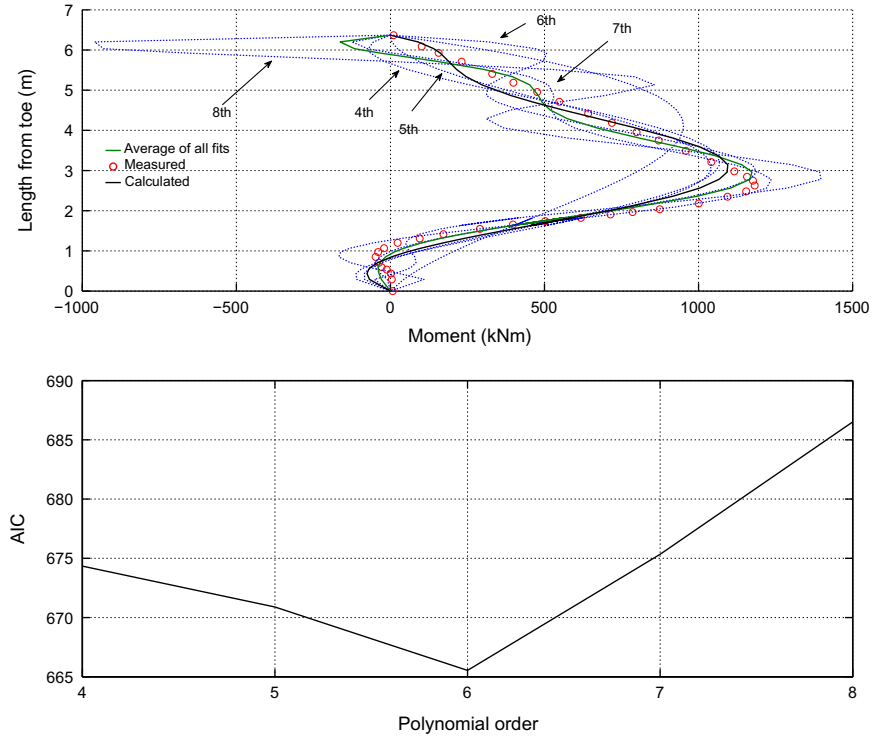

Fig. 3. Development of method for Reese (1997) (a) Polynomial choice and (b) AIC.

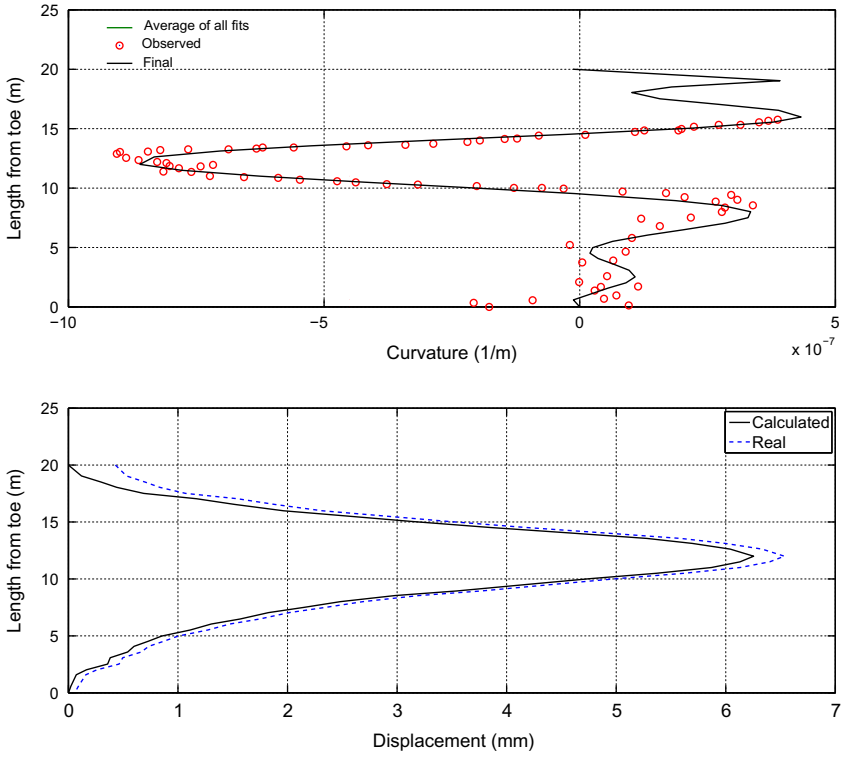

Fig. 4. Calculation (a) curvature and (b) input displacement – Mohamad et al. (2011).

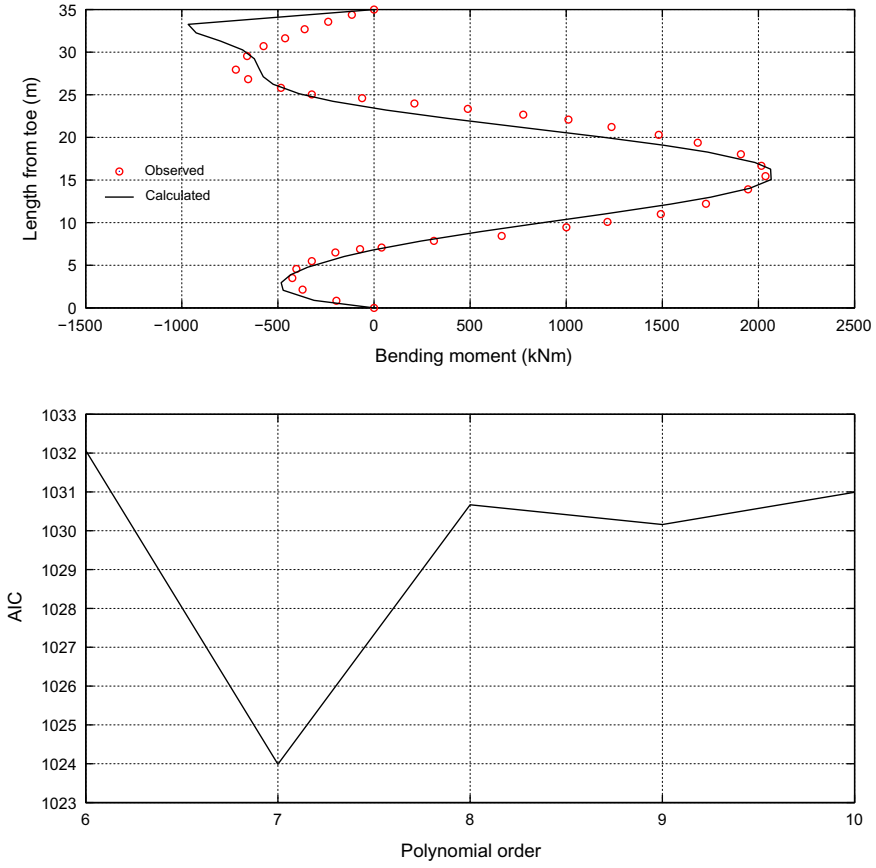

Fig. 5. Calculation (a) bending moment, (b) input displacement – Ou et al. (1998).

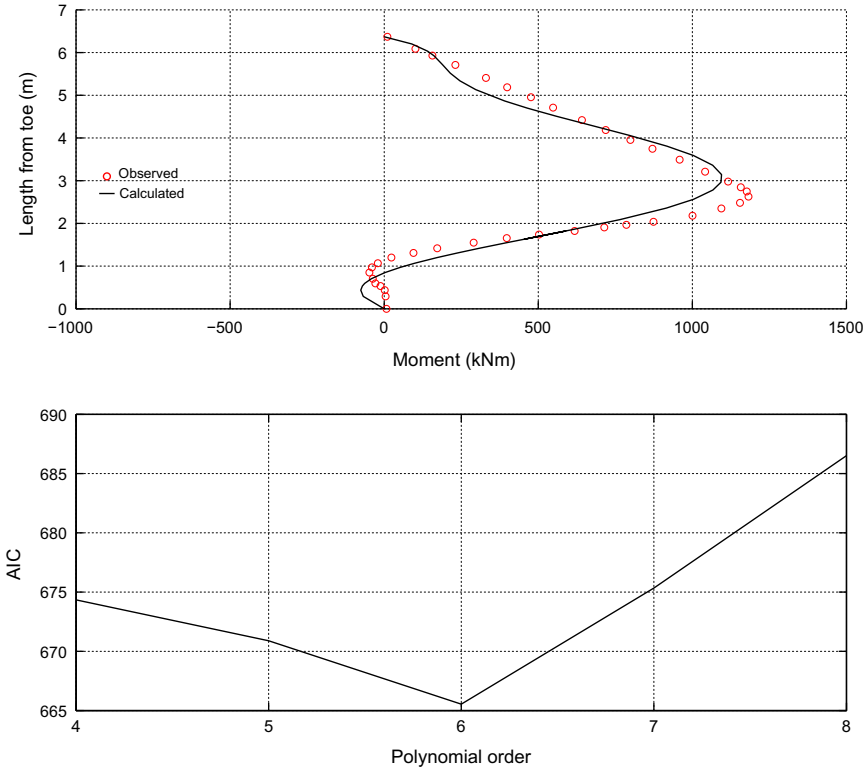

Fig. 6. Calculation (a) bending moment and (b) input displacement – Reese (1997).

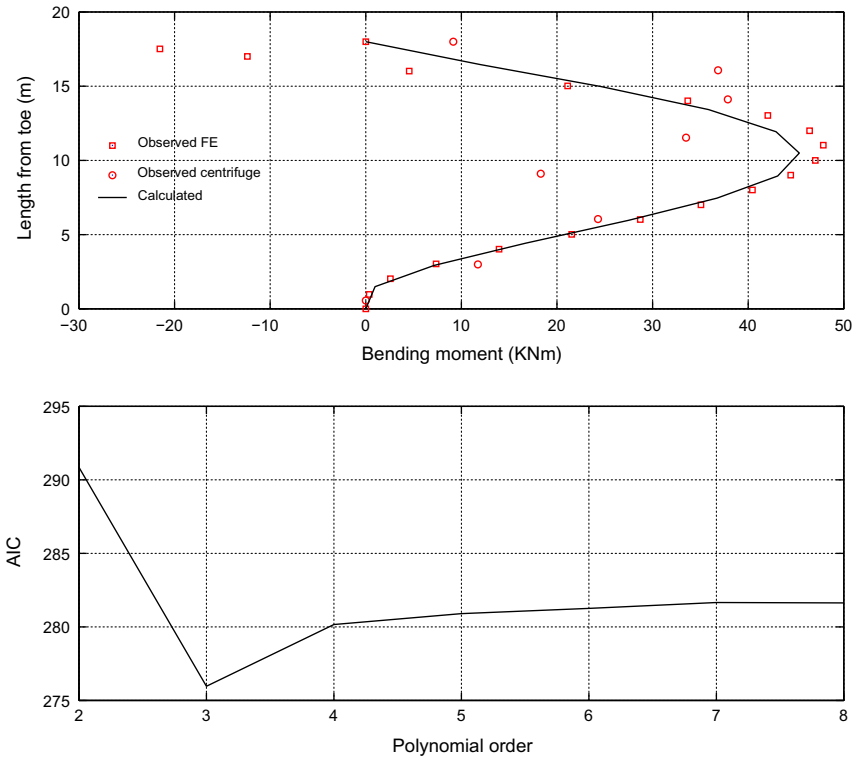

Fig. 7. Calculation (a) bending moment and (b) input displacement – Cheng et al. (2007).

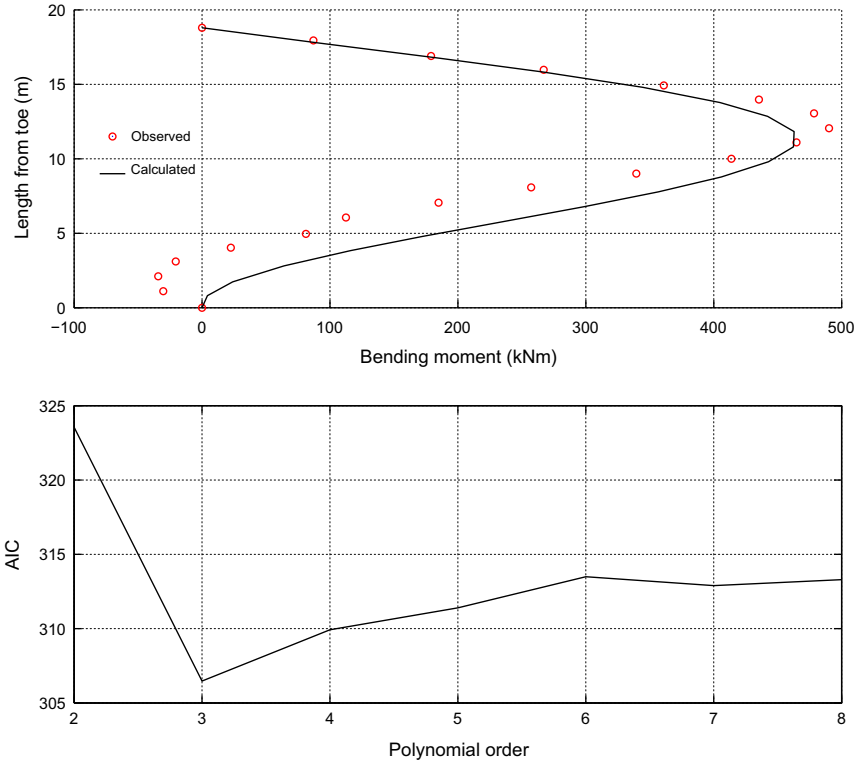

Fig. 8. Calculation (a) bending moment and (b) input displacement – Liyanapathirana and Poulos (2005).

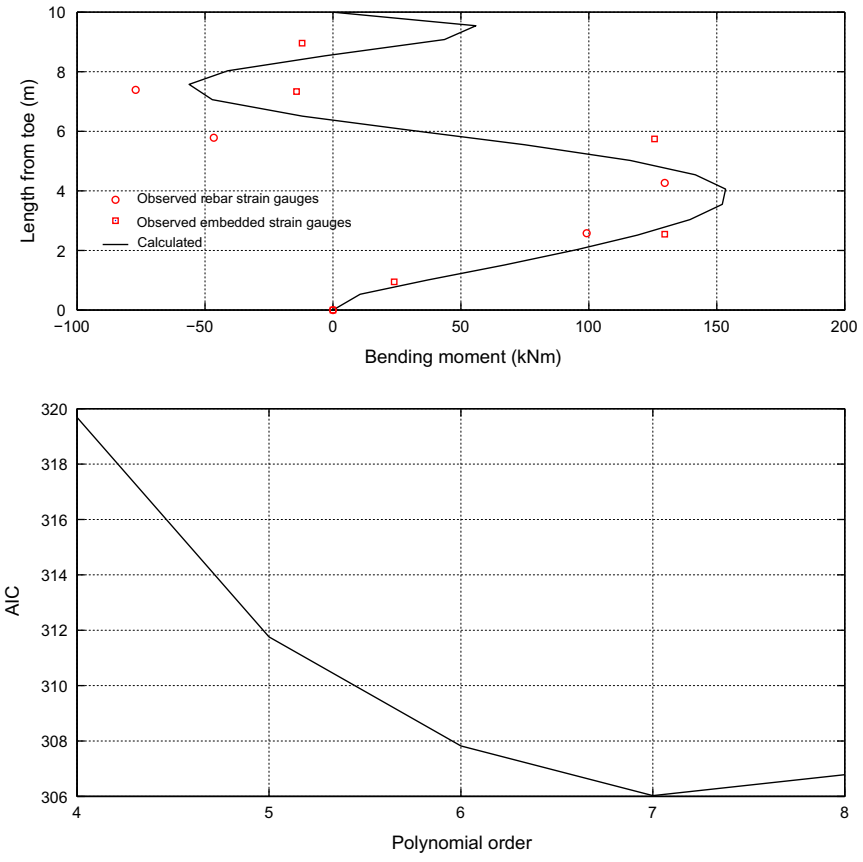

Fig. 9. Calculation (a) bending moment and (b) input displacement – Smethurst and Powrie (2007).

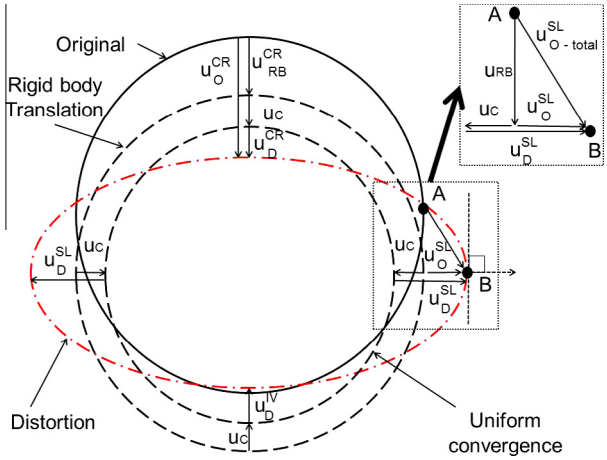

Fig. 10. Tunnel displacements definitions.

corresponds to the highest or lowest polynomial order considered initially, it will be necessary to reduce or increase the order until the minimum is found.

– Once the best order has been chosen, the final solution is taken as the average of fits between the optimal polynomial order and the two closest orders with the lowest AIC score. It must be noted that the two closest may be on one side of the optimal. For example, in Mohamad et al. (2011), the optimal order is 9th and 10th and 11th have lower AIC scores than 8th. Hence, the final solution is taken as the average of polynomials of orders 9th, 10th and 11th.

The above strategy was tested for all the cases in Table 1 as part of the validation process below. Appendix A shows its full application, including AIC plots for all the cases.

4.4. Validation

Six case studies (described in Table 1) were analysed to validate the method's application to piles and embedded retaining walls. They portray multiple loading conditions (earth pressures, tunnel induced load on piles, earthquake induced loads on piles, to piles embedded in sliding embankments), structural dimensions and construction methodologies and hence, cover a wide spectrum of situations.

Figs. 4–9 show comparisons between the Calculated values (resulting from the method's application) and the Observed values (obtained from the literature). The figures also show the Input displacement and the Observed values to illustrate in which cases a transformation, like that shown in Fig. 1d, was needed to calculate u_D.

The match between the maximum Observed values from the literature and the Calculated is within 10% for all cases, with the exception of Smethurst and Powrie (2007), which is 18%. It must be noted that in this case the value of EI that was used is only an estimate by the authors for a stage where the pile is no longer behaving fully elastically. It therefore confirms the potential of the method to predict bending moments beyond the elastic range if the adequate value of EI is used.

The Calculated values deviate, in some instances (e.g. Ou et al., 1998) towards the ends of the structure, typically, the upper part, which corresponds to where the displacement readings, mostly done by inclinometers, accumulate the highest errors. Therefore, this source of deviation cannot be simply attributed to the method as it is more likely to be mostly due to inaccuracies in displacement measurements.

5. Application to tunnels

5.1. Assumptions

The same general assumptions used for piles and retaining walls apply to tunnels. Here, the focus is on circular tunnels for simplicity, although the same principles apply to other section shapes. It is assumed that the tunnel lining structure is monolithic (i.e. the joints are not articulated) and provides full structure continuity.

Furthermore, it is assumed that the ratio between the radius of the tunnel and its lining thickness is greater than 7 approximately and therefore, the beam can be analysed using straight beams deflection theory (Roark, 1965) – i.e. Eq. (2) applies. This assumption also allows disregarding the effect of shear forces, as the structure can be considered a thin shell.

Radial displacements, perpendicular to the tunnel cross section, were used (see Fig. 10). The Observed displacements (u_O) can be, as in piles and retaining walls, divided into two categories: those that produce bending moments and those that do not. The latter, in practice, are rigid body (u_{RB}) displacements – i.e. a translation and/or rotation – and uniform convergence (u_C) displacements – i.e. a uniform reduction in the tunnel diameter (see Fig. 10). The former are displacements referred here as distortion displacements (u_D) – typically ovalisation; however, other potential

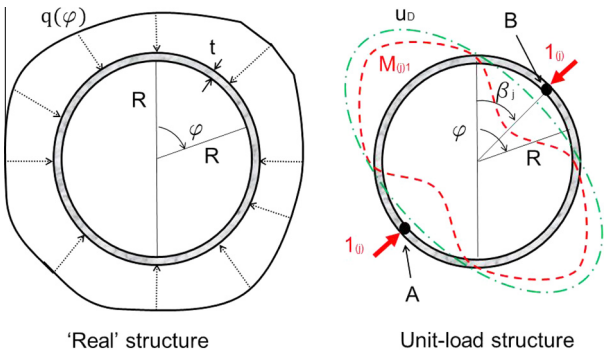

Fig. 11. Tunnel nomenclature definition and idealisation and unit-load structure.

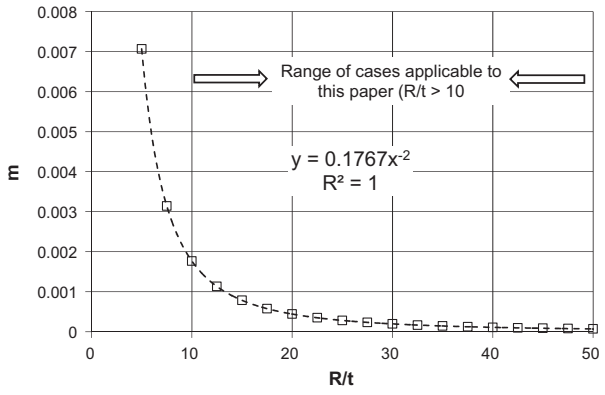

Fig. 12. Ratio between axial force and bending moment contributions to radial displacements.

displacements such as those arising from gaps behind the lining or localised loading must also be included (the example shows only ovalisation deformations for simplicity). It is important to note that everything that follows applies to the rotated tunnel, which means that if a rigid body rotation has occurred, it needs to be removed from the observed values in advance to present it as it is shown in Fig. 10.

Having made the above distinction, the general equation for the radial displacements can be written as

$$u_O = u_{RB} + u_C + u_D \tag{14}$$

where u_O represents the Observed radial displacements of the rotated tunnel and u_{RB} is the projection of the rigid body displacement onto the radial direction for each point (e.g. if the rigid body displacement is a vertical translation as in Fig. 10, the tunnel crown u_{RB} is the Observed total rigid body displacement value, whereas in the springline this value is zero). The sign convention in Eq. (14) is: negative for radial displacements acting inwards and positive for those acting outwards.

The uniform convergence and rigid body displacements do not cause a change in shape (i.e. the normal to tunnel lining does not change direction), which means there is no shear deformation, and no bending moment. Therefore, if the normal to the tunnel at the springline remains horizontal after deformation, it follows that the distortion displacement at this location must also be horizontal. It also means that the vertical component of the rigid body displacement is equal to the vertical component of the observed displacement. Hence, if the same horizontal component of the observed displacement applies at both springlines and in opposite directions, the rigid body displacement must be vertical (as is the case presented in Fig. 10). This reasoning applies to any tunnel as long as the lining acts as a monolithic material with no joints.

Uniform convergence can be obtained by inspecting the tunnel cross section displacements at the crown (CR) and the springline (SL) and developing (14) for each

$$u_O^{SL} - u_{RB}^{SL} = u_C + u_D^{SL} \tag{15}$$

$$u_O^{CR} - u_{RB}^{CR} = u_C + u_D^{CR} \tag{16}$$

In Fig. 10, the distortion deformation of the example is elliptical and therefore, Eq. (15) refers to displacements in the horizontal direction and (16) in the vertical direction.

Using the ratio between the crown and springline distortion deformations, u_D^{CR}/u_D^{SL}, substituting this into Eqs. (15) and (16), subtracting algebraically both eliminates u_C, and isolating u_D^{SL} results in

$$u_D^{SL} = \frac{u_O^{SL} - u_{RB}^{SL} - u_O^{CR} + u_{RB}^{CR}}{(1 - u_D^{CR}/u_D^{SL})} \tag{17}$$

and inserting (17) into (15) provides the uniform convergence

$$u_C = u_m^{SL} - u_{RB}^{SL} - \frac{u_O^{SL} - u_{RB}^{SL} - u_O^{CR} + u_{RB}^{CR}}{(1 - u_D^{CR}/u_D^{SL})} \tag{18}$$

This value can then be used in Eq. (14) to calculate the final distortion displacements at any point in the lining

$$u_D = u_O - u_{RB} - u_O^{SL} + u_{RB}^{SL} + \frac{u_O^{SL} - u_{RB}^{SL} - u_O^{CR} + u_{RB}^{CR}}{(1 - u_D^{CR}/u_D^{SL})} \tag{19}$$

Other methods can be used to separate sources of Observed displacements. What is important is to make sure that all displacements that do not produce bending moments are removed in

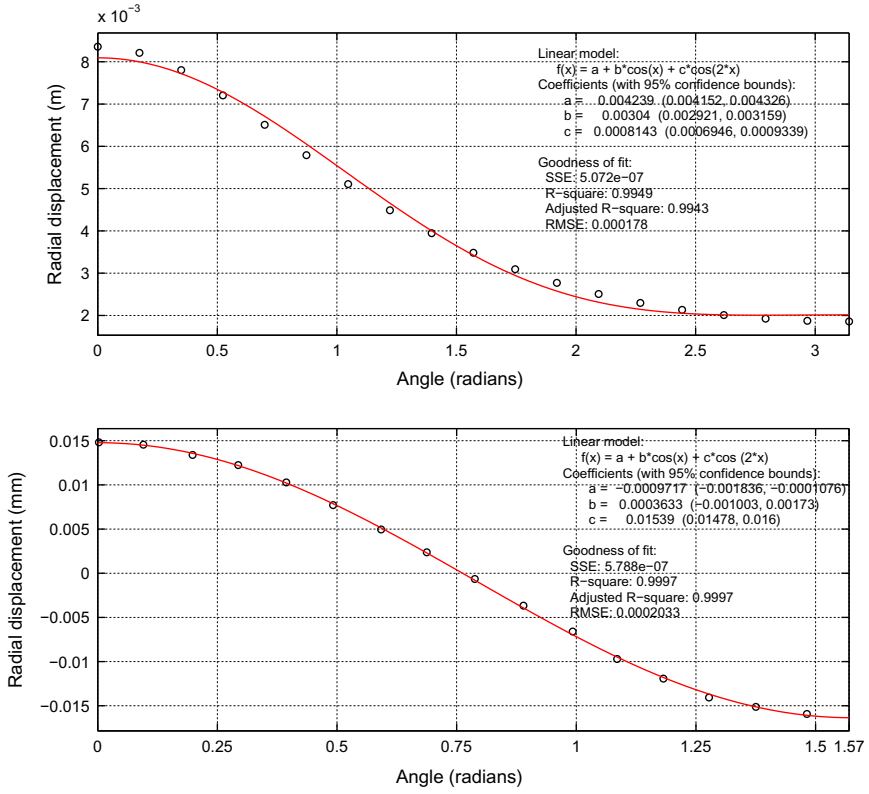

Fig. 13. Validation of function choice (a) Gonzalez and Sagaseta (2001) and (b) Carranza-Torres et al. (2013).

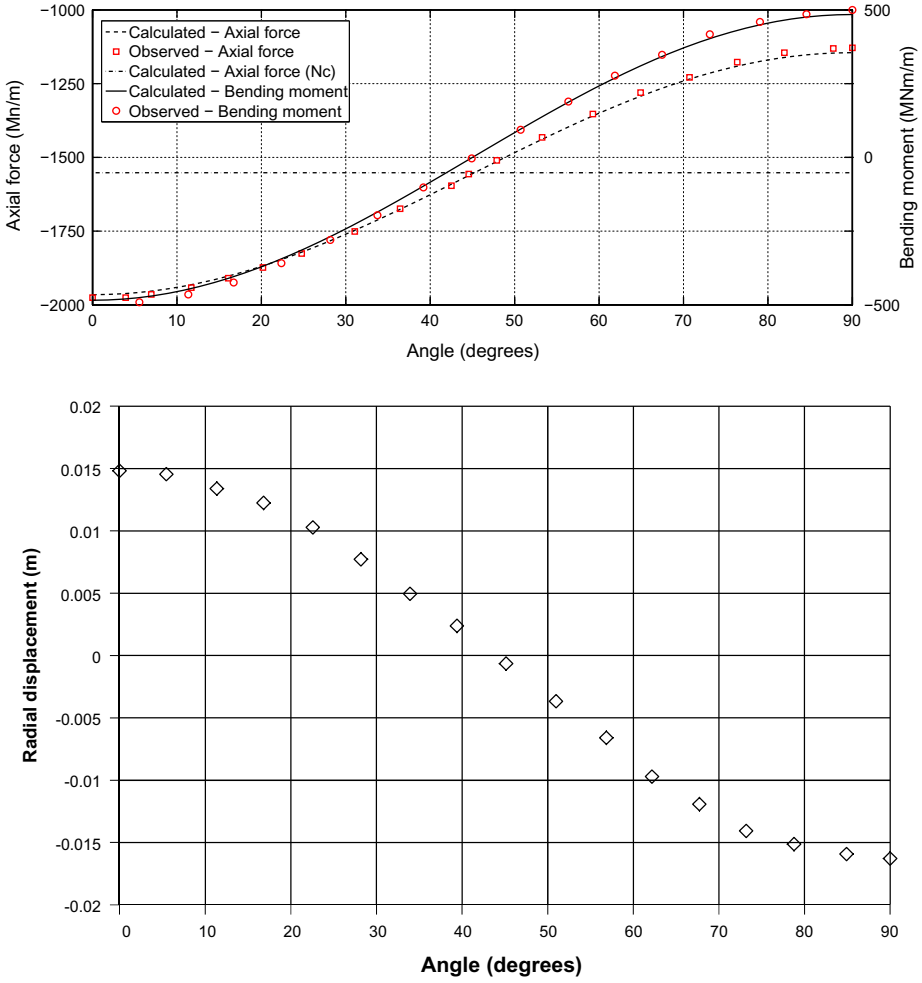

Fig. 14. Calculation of (a) bending moment and Axial force and (b) input radial displacement – Carranza-Torres et al. (2013).

preparation for the method's application. However, the methodology presented here is deemed applicable to most cases of standard displacements in tunnels and has been validated.

The idealisation needed for the application of the method to tunnels is shown in Fig. 11. It consists of a thin ring with a double unit-load applied in diametrically opposite locations.

5.2. Formulation

The chosen function to represent the real structure bending moments and axial forces is shown below

$$f_0(x) = 1, f_1(x) = \cos(\varphi), f_2(x) = \cos(2\varphi) \tag{20}$$

which is much simpler than for piles and retaining walls as it contains only three constants C (see Eq. (6)) to calculate.

The distribution of bending moments for a generic unit-load system applied at an angle β_j was calculated generically for any angle φ, using the equations developed by Lundquist and Burke (1936)

$$M_{(j)1}(\varphi) = \begin{cases} X_{(j)m} + R(1-\sin(\varphi))X_{(j)p} + R\sin(\varphi)X_{(j)v}, & \varphi < \beta_j \\ R\sin(\varphi-\beta_j) + X_{(j)m} + R(1-\sin(\varphi))X_{(j)p} + R\sin(\varphi)X_{(j)v}, & \varphi \geqslant \beta_j \end{cases} \tag{21}$$

where φ varies between 0° and 180°, and

$$X_{(j)m} = R\frac{\left(\frac{\pi\sin(\beta_j)}{2}+2\right)-3}{\pi} \tag{22}$$

$$X_{(j)p} = \frac{2-\left(\frac{\pi\sin(\beta_j)}{2}+2\right)}{\pi} \tag{23}$$

$$X_{(j)v} = \frac{\cos(\beta_j)}{2} \tag{24}$$

Using Eqs. (20)–(24), similar equations to (10) and (11) can be derived for tunnels as follows

$$B_{j,0} = \pi X_{(j)m} + \pi R X_{(j)p} - 2RX_{(j)v} + R(\cos(\beta_j)+1) \tag{25}$$

$$B_{j,1} = X_{(j)m}\sin(\beta_j) - X_{(j)p}R\frac{\sin(2\beta_j)}{2} - \frac{R\sin(\beta_j)(\pi-\beta_j)}{2} \tag{26}$$

$$B_{j,2} = \frac{2}{3}RX_{(j)v} - \frac{R}{3}(\cos(\beta_j)+1)(2\cos(\beta_j)-1) \tag{27}$$

which allows redefining Eq. (6)

$$u_{Dj} = \frac{R}{EI}\sum_{i=1}^{n+1} B_{ij}C_{i-1} \tag{28}$$

that represents the system equations from which the bending moments' constants of Eq. (20) can be calculated.

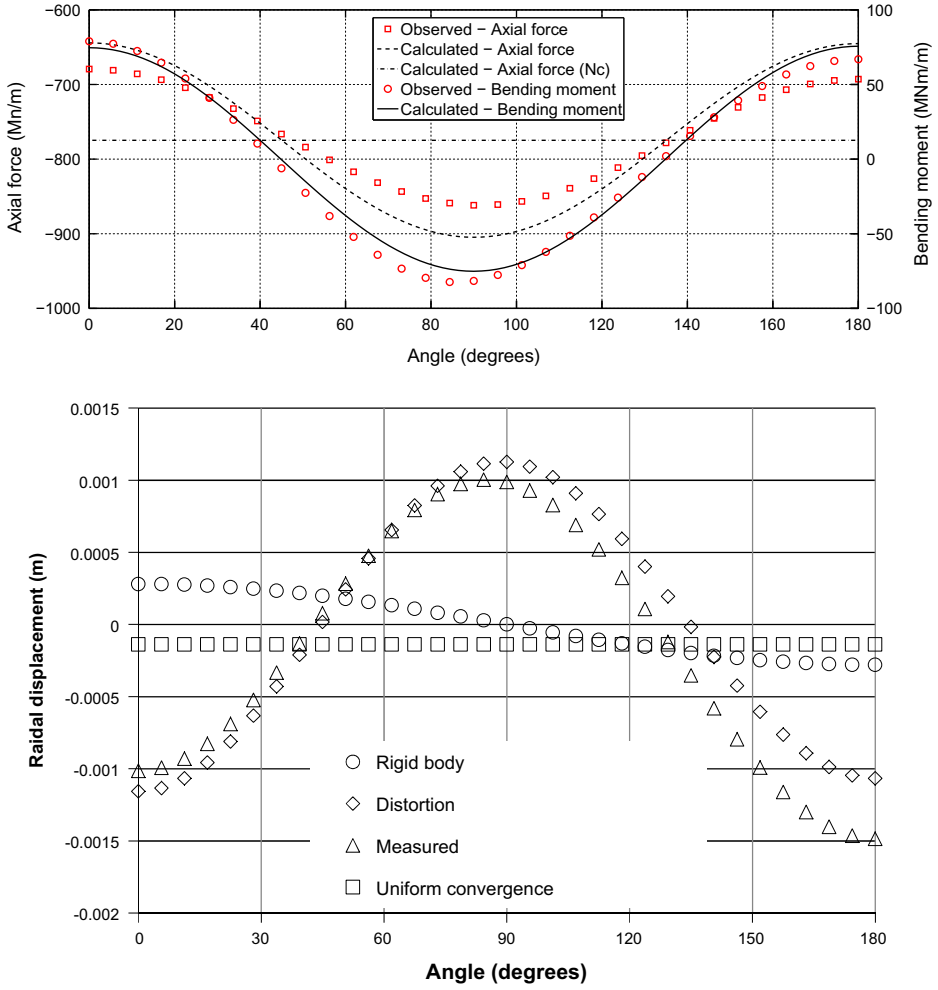

Fig. 15. Calculation of (a) bending moment and Axial force and (b) input displacements – Brinkgreve et al. (2011).

Eqs. (6) and (28) are almost identical with the exception of the addition of R in the latter, which comes from the integration using polar coordinates and the angle φ.

The same process applies to the axial force. In this case, the axial force caused by the unit-load is

$$N_{(j)1}(\varphi) = \begin{cases} -\frac{1}{2}sin(\beta_j - \varphi), & \varphi < \beta_j \\ -\frac{1}{2}sin(\varphi - \beta_j), & \varphi \geqslant \beta_j \end{cases} \tag{29}$$

Using Eqs. (20) and (29), the integrals in (6) become

$$B_{j,0} = 1 \tag{30}$$

$$B_{j,1} = (2\beta_j - \pi)/4 \tag{31}$$

$$B_{j,2} = -(2\cos^2\beta_j - 1)/6 \tag{32}$$

and the system of equations is defined as

$$mu_{Dj} = \frac{R}{EA}\sum_{i=1}^{n+1} B_{ij}C_{i-1} \tag{33}$$

The factor m shown in (33) represents the fact that only a marginal contribution of the distortion movements applies to the axial forces. The majority of the axial force is a consequence of the displacement u_C and can be calculated as

$$N_C = \frac{(R + u_C) - R}{R}\mathrm{EA} = \frac{u_C}{R}\mathrm{EA} \tag{34}$$

So that the final axial load is the summation of N_C (which is a constant load) and the axial load calculated using Eq. (33) that varies for different points in the lining.

The factor, m, can be estimated ignoring the contribution of the shear forces and using the radial displacement solution presented by Gere and Timoshenko (1987)

$$u_D = \frac{\pi PR}{4EA}\left(12\left(\frac{R}{t}\right)^2 + 2.12\right) \tag{35}$$

The second term of the equation corresponds to the axial force contribution, and the first to the bending moments. Fig. 12 shows the power law that fits perfectly the ratio between both contributions, m, when plotted against R/t ratio. Although Eq. (35) and consequently, Fig. 12, correspond to the case of a point load applied at the crown of the lining, other combinations of external applied loads result in very similar power laws and hence, the hypothesis was that the power law presented here can be used for estimation purposes where the deformation of the tunnel is mainly elliptical. This hypothesis is validated below for both case studies.

5.3. Choice of function f(x)

Most of the widely accepted solutions for tunnel lining design define the shape of bending moments and radial displacements in tunnels using multiples of the cosine – e.g. $\cos(2\varphi)$ (Einstein & Schwartz, 1979; El Naggar et al., 2008; Carranza-Torres et al., 2013) for simpler modes of deformation and $\cos(p\varphi)$ for different orders, where p is an integer greater than 1 (Muir Wood, 1975).

Gere and Timoshenko (1987) showed that the equation linking radial displacement and bending moment of a circular beam of thin section is

$$\frac{d^2u_D}{d\varphi^2} + u_D = -\frac{R^2M(\varphi)}{EI} \tag{36}$$

which means that it is mathematically proven that if a function shape of the form shown in (20) could be successfully fitted to the displacement profile u_D, the same form would apply to the bending moments, provided that EI remains constant (as it does for the linear elastic region under consideration).

Fig. 13 shows the fitted proposed function in Eq. (20) to the displacement profiles suggested by Gonzalez and Sagaseta (2001) and Carranza-Torres et al. (2013) using the MATLAB (2013) curve fitting tool. The former presents a profile where symmetry occurs around the vertical axis (note the x axis extends to 180°), whereas in the latter, double symmetry occurs at 90° and subsequently at 180°.

Besides the discussion on the appropriateness of one method or another, which is beyond the scope of this paper, the figure shows that the chosen function performs well for both cases and provides very high values of R^2 and low of RMSE, indicating an acceptable goodness-of-fit. This, in turn, shows that the function is also appropriate to characterise bending moments: a similar rationale applies to axial forces.

5.4. Validation

The validation was carried out against an analytical method such as Carranza-Torres et al. (2013) and an FE model in Brinkgreve et al. (2011). The former is a more generalised and complex case than those presented previously by others others (e.g. Einstein & Schwartz, 1979) and includes complex processes such as stress relaxation. The second case is representative of an accurate and calibrated FE model and programme widely used. Details on both of these are presented in Table 1.

In order to separate the displacements, first an estimate of u_D^{CR}/u_D^{SL} is needed. In cases where the rigid body translation is small compared to the maximum distortion deformations (as is the case in most tunnels), it can be estimated as u_O^{CR}/u_O^{SL}. Hence, u_D^{CR}/u_D^{SL} values of −1.027 and −1.099 were estimated for Brinkgreve et al. (2011) and Carranza-Torres et al. (2013) respectively. This estimate was tested through a sensitivity analysis of its impact on the calculation of bending moments using the value of pure shear, −0.5, and extreme values ranging between −0.92 and −1.08 (calculated from Roark (1965) for the case of a triangular horizontal pressure applied on the sides). Differences of less than 0.5% in the Calculated bending moment were obtained which confirmed the adequacy of the estimate. Eq. (18) was then used to calculate u_C, providing values of −1.383E−04 m and −6.208E−04 m for Brinkgreve and Carranza-Torres respectively. Finally, Eq. (19) was used to calculate u_D.

Using Eq. (34) and the calculated u_C value, N_C was obtained and was equal to −774.79 kN/m (Brinkgreve et al., 2011) and −1552 kN/m (Carranza-Torres et al., 2013). The m values, were estimated using the equation in Fig. 14, and were 3.460E−03 and 1.767E−03 respectively. This allowed calculating the contribution of u_D that corresponds to the axial forces.

Figs. 14 and 15 present the results of the method's application and its comparison to the observed values. The match to Carranza-Torres et al. (2013) is outstanding as the fit is within 0.5%. For Brinkgreve et al. (2011), the method captures the fact that the bending moment is marginally higher at the crown of the tunnel than at the invert, and only over-predicts the latter by 14%. The Calculated axial force is closer to the Observed values and only shows an error of less than 5% for its maximum values at 0 (and 180) and 90° respectively.

Close inspection of Figs. 14 and 15 also shows that N_C is the arithmetic average of the axial load for both cases and the deviation from this average is the axial load that arises from the displacements mu_D. This deviation is also indicative of the ratio between the vertical and horizontal stresses acting on the tunnel lining, as Carranza-Torres and Diederichs (2009) showed, which may present future opportunities for the estimation of this ratio.

The outstanding performance of the method against very different case studies not only validates it but also the procedure presented for the separation and reasoning of the different displacements contributions.

6. Conclusions

The proposed method is analytically correct and based on the principle of virtual work. It provides a means to calculating internal forces such as bending moments and axial forces without the need for boundary conditions. It solves therefore a long standing problem in underground structures that has significant applications in research and practice as it provides an accurate and independent check on the internal forces in a structure. This is envisaged to allow producing more optimised design though greater understanding of the bending moments and axial forces in underground structures.

The versatility and flexibility of the method has been demonstrated using diverse case studies which shows it is equally applicable to piles, retaining walls and tunnels under multiple loading conditions. The maximum error between Observed and Calculated values of bending moment was lower than 10%, with the exception of the case where slight plastic behaviour occurred and the error was 18%.

The method presents multiple opportunities for future work and its relevance extends beyond underground structures as the same methodology is theoretically applicable to any structure. Therefore, its applicability and potential usage is wide.

Acknowledgments

The author would like to acknowledge the discussions he had and recommendations received from Eden Almog (Arup Tunnelling, London) throughout the derivation of the method from its original idea. It is also acknowledged the suggestions that Loretta von der Tann (University College London and Arup Geotechnics) made on the part dealing with piles and retaining walls and the general presentation of the paper.

Appendix A

This appendix shows the full application of the method to all the case studies presented for piles and retaining walls (see Figs A1–A4).

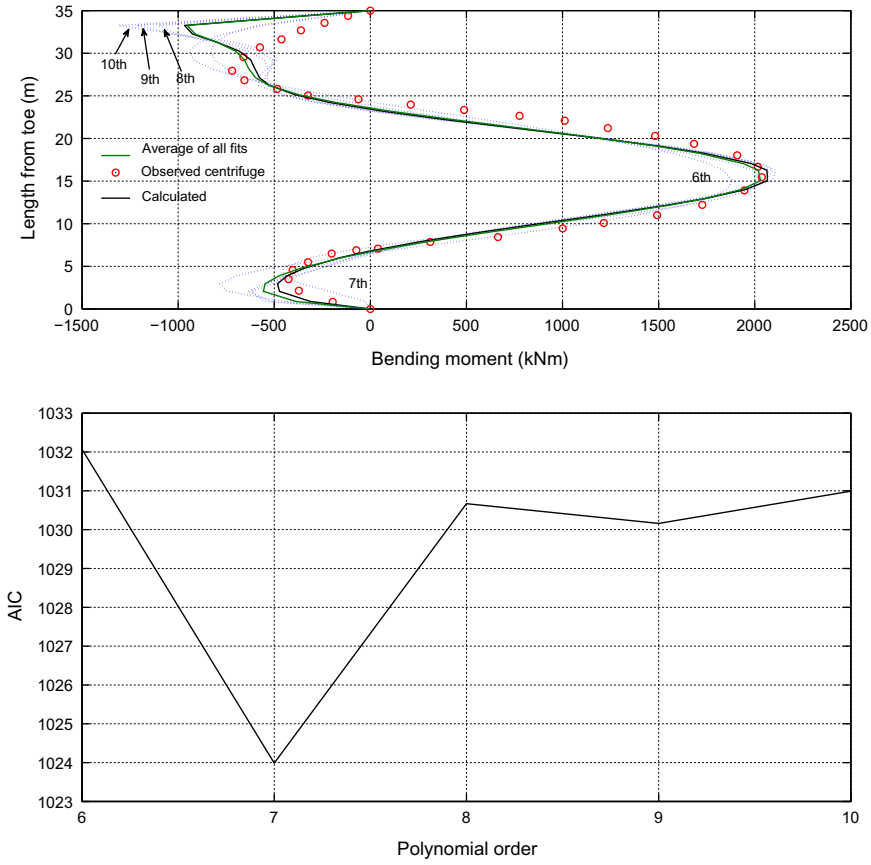

Fig. A1. Development of method for Ou et al. (1998). (a) Polynomial choice and (b) AIC.

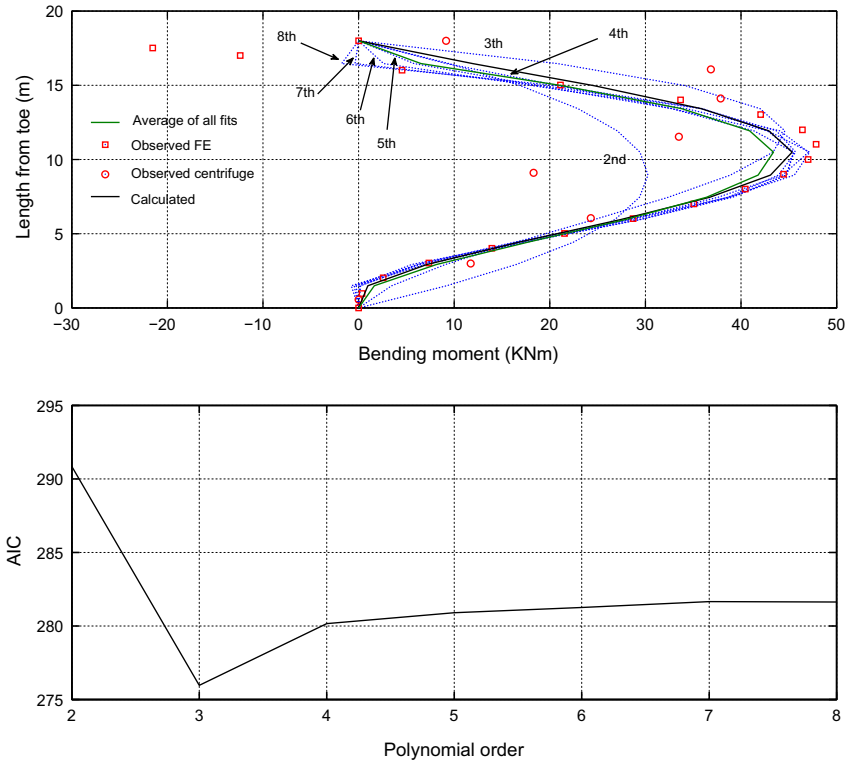

Fig. A2. Development of method for Cheng et al. (2007). (a) Polynomial choice and (b) AIC.

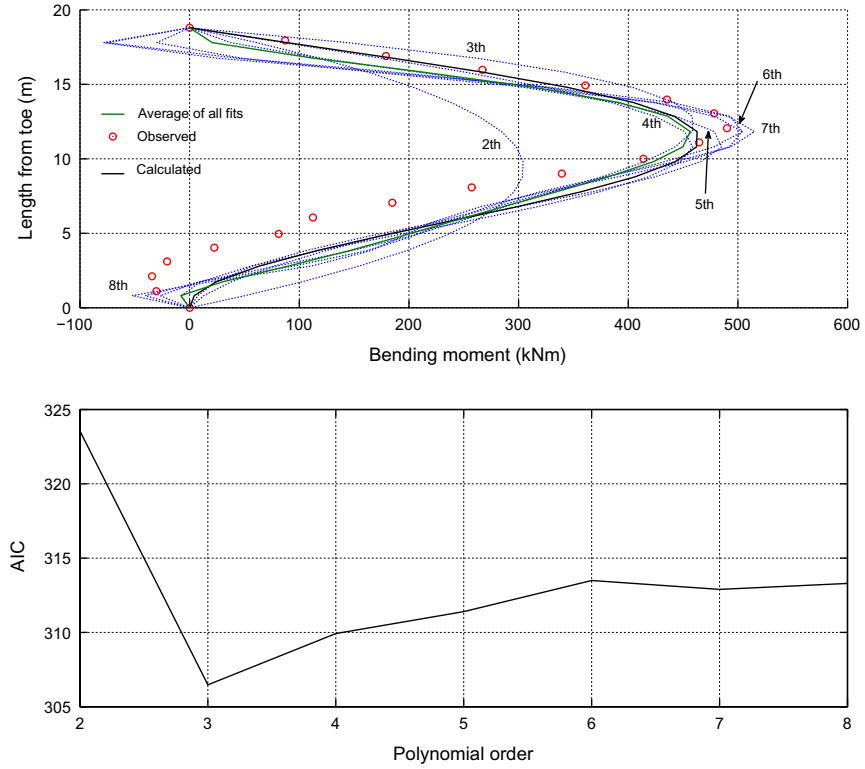

Fig. A3. Development of method for Liyanapathirana and Poulos (2005). (a) Polynomial choice and (b) AIC.

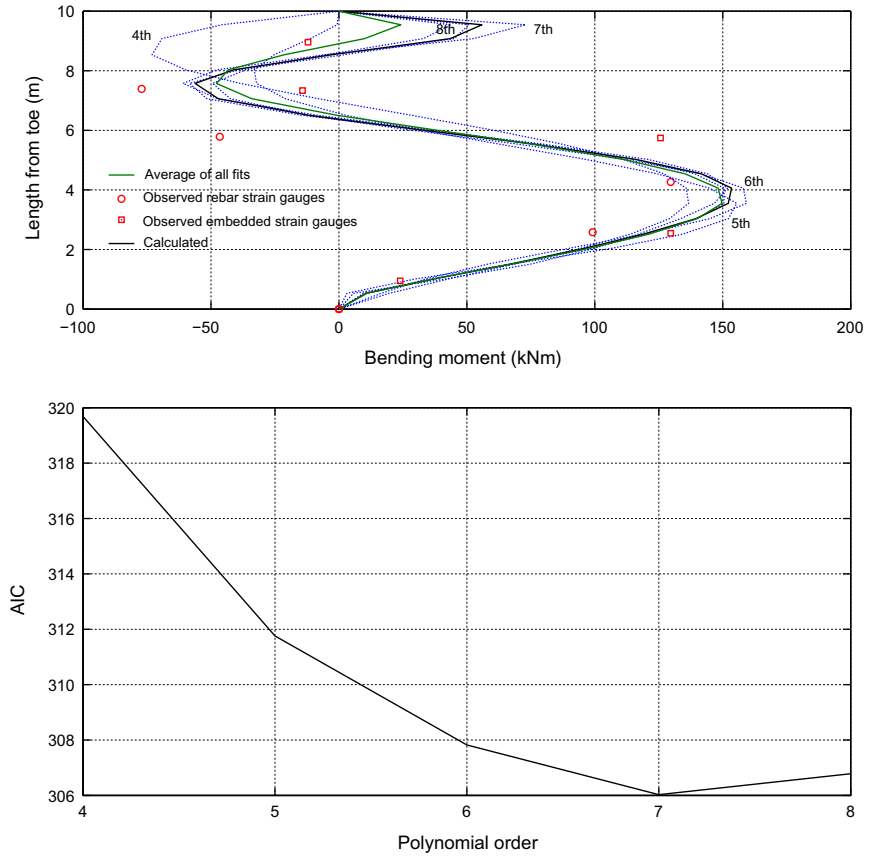

Fig. A4. Development of method for Smethurst and Powrie (2007). (a) Polynomial choice and (b) AIC.

References

Abdoun, T., Dobry, R., O'Rourke, T.D., Goh, S.H., 2003. Pile response to lateral spreads: centrifuge modelling. J. Geotech. Geoenviron. Eng. 129 (10), 869–878.

Anagnostopoulos, C., Georgiadis, M., 1993. Interaction of axial and lateral pile responses. J. Geotech. Eng. 119 (4), 793–798.

Akaike, H., 1974. A new look at the statistical model identification. IEEE Trans. Autom. Control 19 (6), 716–723.

Brown, D.A., Hidden, S.A., Zhang, S., 1994. Determination of p–y curves using inclinometer data. Geotech. Test. J. 17 (2), 150–158.

Brinkgreve, R.B.J., Swolfs, W.M., Engin, E., 2011. Plaxis Introductory: Student Pack and Tutorial Manual 2010. CRC Press, Inc., Boca Raton, FL, USA.

Bozogan, H., 1987. Model selection and Akaike's information criterion (AIC): the general theory and its analytical extensions. Psychometrika 52 (3), 345–370.

Carranza-Torres, C., Rysdahl, B., Kasim, M., 2013. On the elastic analysis of a circular lined tunnel considering the delayed installation of the support. Int. J. Rock Mech. Min. Sci. 61, 57–85.

Carranza-Torres, C., Diederichs, M., 2009. Mechanical analysis of circular liners with particular reference to composite supports. For example, liners consisting of shotcrete and steel sets. Tunn. Undergr. Space Technol. 24, 506–532.

Cheng, C.Y., Dasari, G.R., Chow, Y.K., Leung, C.F., 2007. Finite element analysis of tunnel–soil–pile interaction using displacement controlled model. Tunn. Undergr. Space Technol. 22 (4), 450–466.

Curtis, D.J., 1976. Discussion on Muir Wood. The circular tunnel in elastic ground. Geotechnique 26 (1), 213–237.

de Sousa Coutinho, A., 2006. Data reduction of horizontal load full-scale tests on bored concrete piles and pile groups. J. Geotech. Geoenviron. Eng. 132 (6), 752–769.

Duddeck, H., Erdmann, J., 1985. On structural design models for tunnels in soft soil. Tunnell. Underground Space 9 (5–6), 246–259.

Einstein, H.H., Schwartz, C.W., 1979. Simplified analysis for tunnel supports. J. Geotech. Eng–ASCE 105 (GT4), 499–518.

El Naggar, H., Hinchberger, S.D., Lo, K.Y., 2008. A closed-form solution for composite tunnel linings in a homogeneours infinite isotropic elastic medium. Can. Geotech. J. 45, 266–287.

Fuentes, R., 2012. Study of basement design, monitoring and back-analysis to lead to improved design methods. EngD Thesis, University of London, England.

Gaba, A., Simpson, B., Powrie, W., Beadman, D., 2003. Embedded Retaining Walls: Guidance for Economic Design. Report no 580. CIRIA. London.

Gere, J.M., Timoshenko, S.P., 1987. Mechanics of Materials, 2nd SI ed. Van Nostrand Reinhold (UK) Co., Ltd.: UK.

Gonzalez, C., Sagaseta, C., 2001. Patterns of soil deformations around tunnels. Application to the extension of Madrid Metro. Comput. Geotech. 28, 445–468.

Hurvich, C.M., Tsai, C.-L., 1991. Bias of the corrected AIC criterion for underfitted regression and time series models. Biometrika 78 (3), 499–509.

Inaudi, D., Vurpillot, S., Casanova, N., Kronenberg, P., 1998. Structural monitoring by curvature analysis using interferometric fibre optic sensors. Smart Mater. Struct. 7, 199–208.

International Tunnelling Association – ITA, 1988. Working group on general approaches to the design of tunnels: Guideliens for the design of tunnels. Tunnell. Underground Space Technol. 3, 237–249.

Kim, S.H., 1996. Model testing and analysis of interactions between tunnels in clays. PhD thesis, University of Oxford, England.

Liyanapathirana, D.S., Poulos, H.G., 2005. Seismic lateral response of piles in liquefying soil. J. Geotech. Geoenviron. Eng. 131 (12), 1466–1479.

Lundquist, E.E., Burke, W.F., 1936. General equations for the stress analysis of rings. Report NACA-TR-509. National Advisory Committee for Aeronautics. <http://naca.central.cranfield.ac.uk/reports/1936/naca-report-509.pdf> (accessed 11.07.14).

Loganathan, N., Poulos, H.G., Stewart, D.P., 2000. Centrifuge model testing of tunnelling-induced ground and pile deformations. Geotechnique 50 (3), 283–294.

MATLAB R2013b (8.2.0.701), 2013. Natick, Massachusetts: The MathWorks Inc.

Mohamad, H., Bennett, P.J., Soga, K., Mair, R.J., Bowers, K., 2010. Behaviour of an old masonry tunnel due to tunnelling-induced ground settlement. Geotechnique 60 (12), 927–938.

Mohamad, H., Soga, K., Pellew, A., Bennett, P.J., 2011. Performance monitoring of a secant-piled wall using distributed fiber optic strain sensing. J. Geotech. Geoenviron. Eng. 137 (12), 1236–1243.

Mohamad, H., Soga, K., Bennett, P.J., Mair, R.J., Lim, C.S., 2012. Monitoring twin tunnel interaction using distributed optical fiber strain measurements. J. Geotech. Geoenviron. Eng. 138 (8), 957–967.

Muir Wood, A.M., 1975. The circular tunnel in elastic ground. Geotechnique 25 (1), 115–127.

Nip, D.C.N., Ng, C.W., 2005. Back analysis of laterally loaded piles. Inst. Civil Eng.: Geotech. Eng. 158 (GE2), 63–73.

Oreste, P.P., 2003. Analysis of structural interaction in tunnels using the convergence- confinement approach. Tunn. Undergr. Space Technol. 18, 347–363.

Ou, C.-Y., Liao, J.-T., Lin, H.-D., 1998. Performance of diaphragm wall constructed using top-down method. J. Geotech. Geoenviron. Eng. 124 (9), 798–808.

Panet, M., Guenot, A., 1982. Analysis of convergence behind the face of a tunnel. In: Proceedings Tunnelling 1982 Conference. London, pp. 197–204.

Reese, L.C., 1997. Analysis of laterally loaded piles in weak rock. J. Geotech. Geoenviron. Eng. 123 (11), 1010–1017.

Roark, R., 1965. Formulas for Stress and Strain, fourth ed. Mc-Graw-Hill Kogakusha.

Smethurst, J.A., Powrie, W., 2007. Monitoring and analysis of the bending behaviour of discrete piles used to stabilise a railway embankment. Géotechnique 57 (8), 663–677.

You, X., Zhang, Z., Li, Y., 2007. An analytical method of shield tunnel based on force method. In: Proceedings of the 33rd ITA-AITES World Tunnel Congress – Underground Space – The 4th Dimension of Metropolises, pp. 791–797.